

1 **Distal ash fall from the mid-Holocene eruption of Mount Hudson (H2)**
2 **discovered in the Falkland Islands: new possibilities for Southern**
3 **Hemisphere archive synchronisation**

4 **Authors**

5 Panayiotis Panaretos^{1,2*}, Paul G. Albert³, Zoë. A. Thomas^{1,2*}, Chris S.M. Turney^{1,2}, Charles R.
6 Stern⁴, G. Jones³, Alan N. Williams^{5,6}, Victoria C. Smith⁷, Alan G. Hogg⁸, Christina J.
7 Manning⁹

8 **Affiliations**

9 ¹ Chronos ¹⁴Carbon-Cycle Facility, Mark Wainwright Analytical Centre, University of New South Wales,
10 Sydney, NSW 2052, Australia

11 ² Earth and Sustainability Science Research Centre (ESSRC), School of Biological, Earth and Environmental
12 Sciences, University of New South Wales, Sydney, NSW 2052, Australia

13 ³ Department of Geography, Faculty of Science and Engineering, Swansea University, Swansea, SA2 8PP,
14 UK

15 ⁴ Department of Geological Sciences, University of Colorado, Boulder, CO, 80309-0399, USA.

16 ⁵ EMM Consulting Pty Ltd, 20 Chandos Street, St Leonards, NSW 2065, Australia

17 ⁶ ARC Centre of Excellence for Australian Biodiversity and Heritage, School of Biological, Earth and
18 Environmental Sciences, University of New South Wales, NSW 2052, Australia.

19 ⁷ Research Laboratory for Archaeology and History of Art (RLAHA), University of Oxford, Oxford, OX1
20 3TG, UK.

21 ⁸ Carbon dating Laboratory, School of Science, University of Waikato, Hamilton, New Zealand.

22 ⁹ Department of Earth Sciences, Royal Holloway University of London, Egham, Surrey, TW20 0EX

23

24 *** Correspondence:**

25 Panayiotis Panaretos - pana.panaretos@gmail.com

26 Zoe Thomas - z.thomas@unsw.edu.au

27 **Abstract**

28 Cryptotephra deposits (microscopic volcanic ash) are important geochronological tools that can be
29 used to synchronize records of past environmental change. Here we report a distal cryptotephra
30 from a Holocene peat sequence (Canopus Hill) in the Falkland Islands, in the South Atlantic. Using
31 geochemical analysis (major- and trace-element) of individual volcanic glass shards, we provide a
32 robust correlation between this cryptotephra and the large mid-Holocene explosive eruption of Mt.
33 Hudson in Patagonia, Chile (H2; ~3.9 ka cal BP). The occurrence of H2 as a cryptotephra in the
34 Falkland Islands significantly increases the known distribution of this marker horizon to more than
35 1200 km from the volcano, a threefold increase of its previous known extent. A high-resolution
36 radiocarbon chronology, based on terrestrial plant macrofossils, dates the H2 tephra to 4265 ± 65
37 cal yr BP, suggesting that the eruption may have occurred slightly earlier than previously reported.
38 The refined age and new geochemical reference dataset will facilitate the identification of the H2
39 tephra in other distal locations. The high concentration of glass shards in our peat sequence
40 indicates that the H2 tephra may extend well beyond the Falkland Islands and we recommend future
41 studies search for its presence across the sub-Antarctic islands and Antarctic Peninsula as a
42 potentially useful chronological marker.

43 **Keywords:** South America, cryptotephra, tephrochronology, Patagonia, Southern Volcanic Zone,
44 Hudson, South Atlantic, Southern Ocean, Antarctic,

45 **1. Introduction**

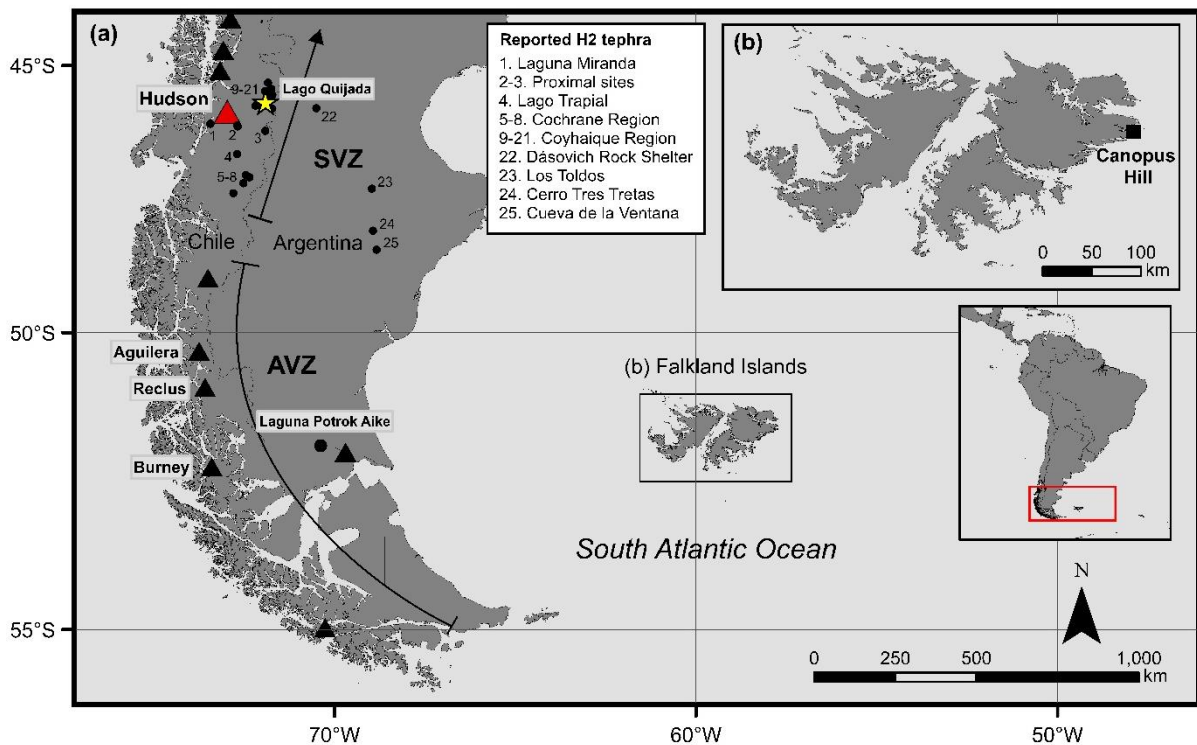
46 Volcanic ash (tephra) dispersed from explosive volcanic eruptions has become a principal
47 geochronological tool for correlating environmental records (e.g., Alloway et al., 2013; Lane
48 et al., 2017). The near instantaneous deposition of tephra over large distances and its often-
49 unique chemical signature allows tephra layers to provide time-parallel marker horizons
50 (isochrones) (Turney and Lowe, 2001). Tephra isochrones can be used to synchronize records
51 of past environmental change between sites and represent one of the most robust and versatile

52 dating methods (Lowe 2011). The application of tephra isochrones has been extended to
53 include microscopic ash deposits (cryptotephra) which have been found in distal areas
54 thousands of kilometres from source volcanoes (e.g., Dugmore, 1989; Wastegård et al., 2000;
55 Dunbar et al., 2017; Kearney et al., 2018; Smith et al., 2020).

56 Despite the value that tephrochronology offers as a powerful geochronological tool, the
57 technique has been underutilized in many regions. One such area is the South Atlantic, a region
58 that owing to the prevailing mid-latitude westerly airflow, is favourably positioned downwind
59 from the major volcanic zones (AVZ and SVZ; Austral and Southern Volcanic Zones) of
60 southern South America (**Fig. 1**). Explosive volcanism is known to have occurred frequently
61 at numerous volcanoes along these zones throughout the Holocene, including Mts. Burney,
62 Aguilera and Reclus within the AVZ and Mt. Hudson in the SVZ (**Fig. 1a**; Stern, 2008; Fontijn
63 et al., 2014). Tephra from these volcanic centres have previously been identified in lakes and
64 peat bogs throughout southern Patagonia (Killian et al., 2003; Weller et al., 2015; Fontijn et
65 al., 2016; Smith et al., 2019). Only a limited number of cryptotephra deposits originating from
66 Patagonian explosive volcanism have previously been reported in peat bogs across the
67 Southern Atlantic, including the Falkland Islands and South Georgia (Hall et al., 2001; Oppedal
68 et al., 2018), with the most recently identified linked to eruptions at Mt. Burney (MB₁; 8.85-
69 9.95 ka cal BP) and the Reclus Volcano (R₁; 14.76 ± 0.18 ka cal BP (Monteath et al., 2019;
70 Stern et al., 2011).

71 Tephrochronology studies in this region offer potential for the alignment of proxy
72 reconstructions investigating climate and environmental change, including Southern
73 Hemisphere westerly wind flow (Kilian and Lamy, 2012; Moreno et al., 2014; Lamy et al.,
74 2010). Unfortunately, few distal tephra (>100 km) have been described in this region and the
75 precise ages and distribution of key marker horizons remain uncertain. Here we present the
76 results of new tephrostratigraphic investigations of the Canopus Hill peat sequence in the

77 Falkland Islands (**Fig. 1b**), with a focus on the provenance and significance of a mid-Holocene
 78 cryptotephra identified in the succession.



79 **Figure 1.** Patagonia in southern South America depicting (a) the volcanoes (triangles) known to have erupted
 80 during the Holocene (Global Volcanism Program 2020) from the Austral and Southern Volcanic Zones as defined
 81 by Stern (2004). (b) Location of the Falkland Islands and study site at Canopus Hill. Black dots represent locations
 82 where H2 tephra has been reported (**Table S1**). (1) Haberle and Lumley, 1998; (2-3) Naranjo and Stern, 1998; (4)
 83 Fagel et al., 2017; (5-8) Stern et al., 2016; Fagel et al., 2017; (9-21) Weller et al., 2015; Markgraf et al., 2007;
 84 Weller et al., 2018; Elbert et al., 2013; Weller and Stern, 2018; (22) Stern et al., 2019; (23) Cardich, 1984-1985;
 85 (24) Paunero, 1993-1994; (25) Paunero, 2000.

86 **2. Study Area and Methods**

87 **2.1 The Falkland Islands and the Canopus Hill sequence**

88 The Falkland Islands are situated in the South Atlantic, 540 km east of the South American
 89 coast. The islands lie in the central latitudinal belt of the southern westerly winds (SWW) and
 90 have high monthly and annual windspeeds ($6-9 \text{ ms}^{-1}$) (Upton and Shaw, 2002; Clark and
 91 Wilson, 1992). Peat bogs cover more than ~85% of the Falkland Islands and are ideal archives

92 to trap and preserve volcanic ash (Otley et al., 2008). The combination of the prevailing airflow
93 and abundance of peat makes the Falkland Islands ideally positioned to receive and preserve
94 tephra from the major volcanic zones in South America (**Fig.1**). Observations of modern
95 volcanic eruptions suggest Patagonian ash fall has been deposited over the Falkland Islands,
96 including ash from the 1991 Hudson eruption plume (Scasso et al., 1994; Kratzman et al.,
97 2010).

98 To investigate the presence of distal cryptotephra, a 1.6 m peat sequence was extracted with a
99 D-section corer from an exposed Ericaceous–grass peatland on Canopus Hill (-51.691° S,
100 57.785 ° W) outside Port Stanley. Previous research at this site recognised the input of exotic
101 pollen and charcoal derived from South America (Turney et al., 2016), as well as a multi-proxy
102 reconstruction of atmospheric circulation changes (Thomas et al., 2018).

103 **2.2 Tephrostratigraphy**

104 The Canopus Hill peat sequence contained no visible tephra layers. The sequence was sampled
105 contiguously every 4 cm. Peat from each interval was ashed at 550°C using an adopted method
106 to concentrate any present cryptotephra (Dugmore, 1989; Pilcher and Hall, 1992). The mineral
107 component was sieved (90 to 25 µm), centrifuged and mounted onto glass slides with Canada
108 balsam. Glass shards were counted using a light microscope. The concentration of volcanic ash
109 shards was determined as shard number per gram of dry sediment. This process was repeated
110 at 1cm intervals where high concentrations of glass shards were detected to determine the exact
111 depth of the cryptotephra peak. The depth interval displaying a peak in volcanic glass shards
112 was then re-sampled and subjected to density separation techniques to isolate the shards (as
113 described in Blockley et al., 2005). The glass shards were then picked using a micromanipulator
114 and bedded into an epoxy resin stub for geochemical characterization.

115 **2.3 Grain-specific major and trace element analysis of tephra**

116 The major element volcanic glass composition of the tephra was determined using a
117 wavelength-dispersive JEOL JXA-8200 electron microprobe at the School of Archaeology,
118 University of Oxford. Full analytical conditions are reported in **Text S1**. All glass data
119 presented has been normalised to 100 wt% for comparative purposes. Error bars on plots
120 represent reproducibility, calculated as a 2x standard deviation of replicate analysis of MPI-
121 DING StHs6/80-G reference glass (Jochum et al., 2006). The full glass dataset of the Canopus
122 Hill cryptotephra and the secondary standard (MPI-DING reference glasses) data are reported
123 in the **Supplementary Dataset**. Trace element analysis of volcanic glass shards from the
124 Canopus Hill cryptotephra, and the Hudson 2 reference ash deposit from Lago Quijada, Chile
125 (see Smith et al., 2019 for details) were performed using an Agilent 8900 triple quadrupole
126 ICP-MS (ICP QQQ) coupled to a Resonetics 193nm ArF excimer laser-ablation in the
127 Department of Earth Sciences, Royal Holloway, University of London. The full analytical
128 conditions are reported in **Text S1**. Full trace element glass datasets for the Canopus Hill
129 cryptotephra and a Hudson 2 reference sample from Lago Quijada are provided in the
130 **Supplementary Dataset**, along with the MPI-DING glass analyses (StHs6/80-G and ATHO-
131 G).

132 **2.4 Chronology**

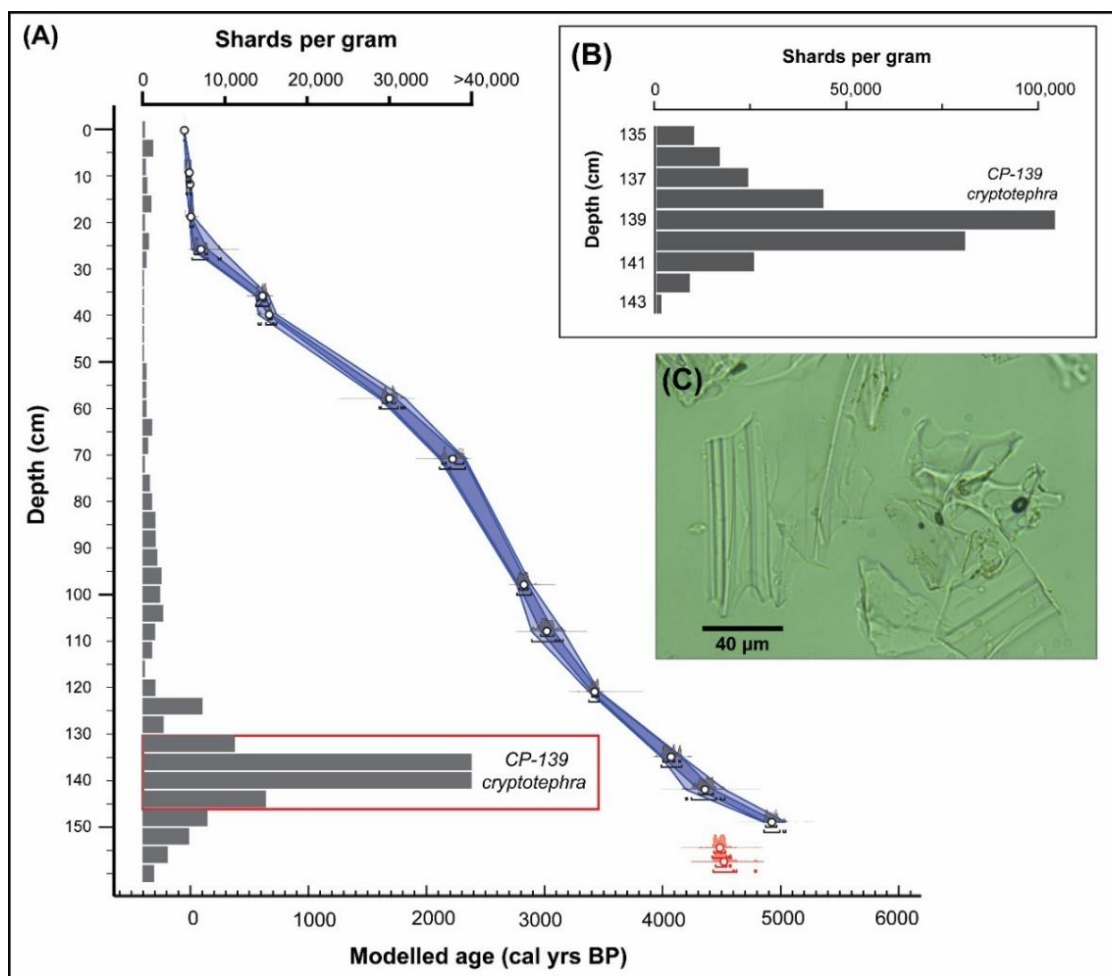
133 Radiocarbon ages for the Canopus Hill peat sequence have previously been published by
134 Thomas et al., (2018). These dates were derived using terrestrial plant macrofossils (fruits and
135 leaves) and were given an acid–base–acid (ABA) pre-treatment. Samples were pretreated,
136 combusted and graphitised in the University of Waikato AMS laboratory, and the $^{14}\text{C}/^{12}\text{C}$
137 measurements were performed at the University of California at Irvine (UCI) on a NEC
138 compact (1.5SDH) AMS system. The ^{14}C measurements were supplemented by ^{137}Cs
139 measurements near the top of the profile to detect the onset of nuclear tests in the mid- 20th

140 century. An additional macrofossil sample (graminoid fragments) was extracted for ^{14}C dating
141 from the sequence at 134 cm, to help constrain the existing age-depth model. The macrofossil
142 was pre-treated, graphitised and measured on an Ionplus MICADAS at the University of New
143 South Wales Chronos ^{14}C Carbon-Cycle Facility (Turney et al., in press). The additional ^{14}C date
144 was added to the Bayesian age depth model and re-calibrated using SHCal20 (Hogg et al.,
145 2020) and Bomb13SH1-2 (Hua et al, 2013). All radiocarbon ages for Canopus Hill are provided
146 in **Table S2**.

147 **3. Results and discussion**

148 **3.1 Tephrostratigraphy**

149 Volcanic glass was found in varying abundances throughout the Canopus Hill sequence. Most
150 shards were clear and appeared light pink, but a smaller proportion were darker. A distinct peak
151 in volcanic glass occurred within the 136-140 cm and 140-144 cm intervals of the peat
152 sequence (**Fig. 2a; Fig S1**). These intervals contained very high concentrations (>40,000 shards
153 per gram) of clear/light pink volcanic glass shards. Further examination at 1 cm resolution
154 indicated the peak in glass shards occurred between 139-140 cm (**Fig 2b.**). The morphology of
155 the shards at 139 cm were predominantly formed of clear, platy and cusped shards. The age
156 depth model for the Canopus Hill sequence, indicates the age of this cryptotephra deposit is
157 4265 ± 65 cal yrs BP (**Fig 3**), based off the midpoint of the cryptotephra at 139.5 cm.



158

159 **Figure 2.** Tephrostratigraphy of the Canopus Hill sequence. (A) Glass shard concentrations of samples spanning
 160 4 cm intervals from 0-164 cm and the updated age depth model for the Canopus Hill peat sequence (Thomas et
 161 al., 2018). The P_sequence and “outlier analysis” options were used to develop the age depth model in OxCal 4.4
 162 (Bronk Ramsey, 2008; Bronk Ramey, 2009; Bronk Ramsey and Lee, 2013; Bronk Ramsey, 2017). (B) The glass
 163 shard concentrations between 135-143 cm at 1 cm intervals. (C) Image of volcanic shards from the CP-139
 164 cryptotephra (light microscope, 20x magnification).

165 3.2 Geochemical characterization and origin of the CP-139 cryptotephra

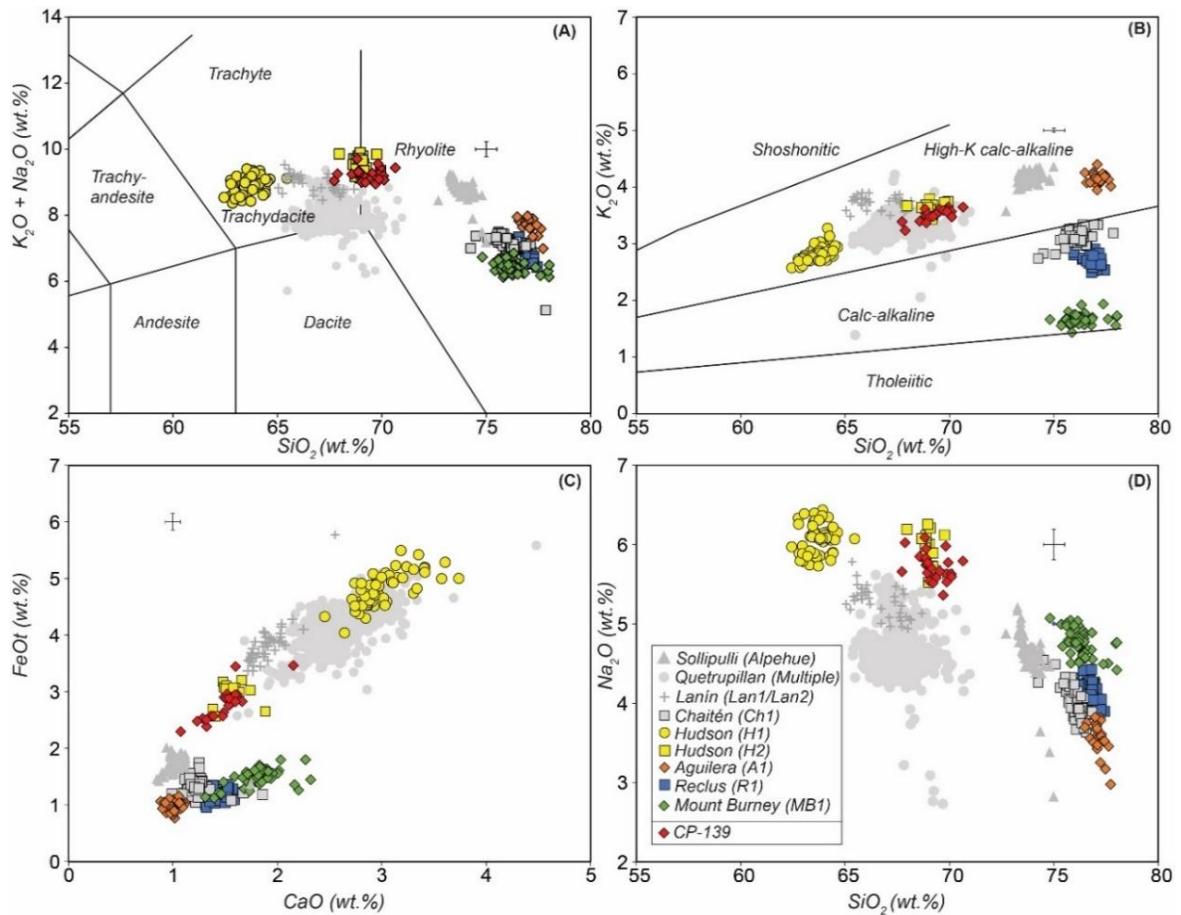
166 The CP-139 cryptotephra has a relatively heterogeneous volcanic glass composition that
 167 straddles the trachydacite-rhyolite boundary (67.3-70.6 wt.% SiO₂; 8.9-9.7 wt.% Na₂O+K₂O;
 168 **Fig. 3a**). These volcanic glasses also display a High-K calc-alkaline affinity (HKCA; 3.2-3.6
 169 wt.% K₂O). Using increasing SiO₂ as a fractionation index, the CP-139 glasses display a clear
 170 decrease in TiO₂, FeO_t, MgO and CaO contents, whilst the K₂O content increases.

171 Incompatible trace element contents of the CP-139 glasses reveal minor heterogeneity (e.g.,
172 458-534 ppm Zr; 40-46 ppm Y; 891-946 ppm Ba) and show Light Rare Earth Element (LREE)
173 enrichment relative to the Heavy Rare Earth Elements (HREE) ($\text{La/Yb} = 9.6 \pm 4.7$ [2.s.d]).

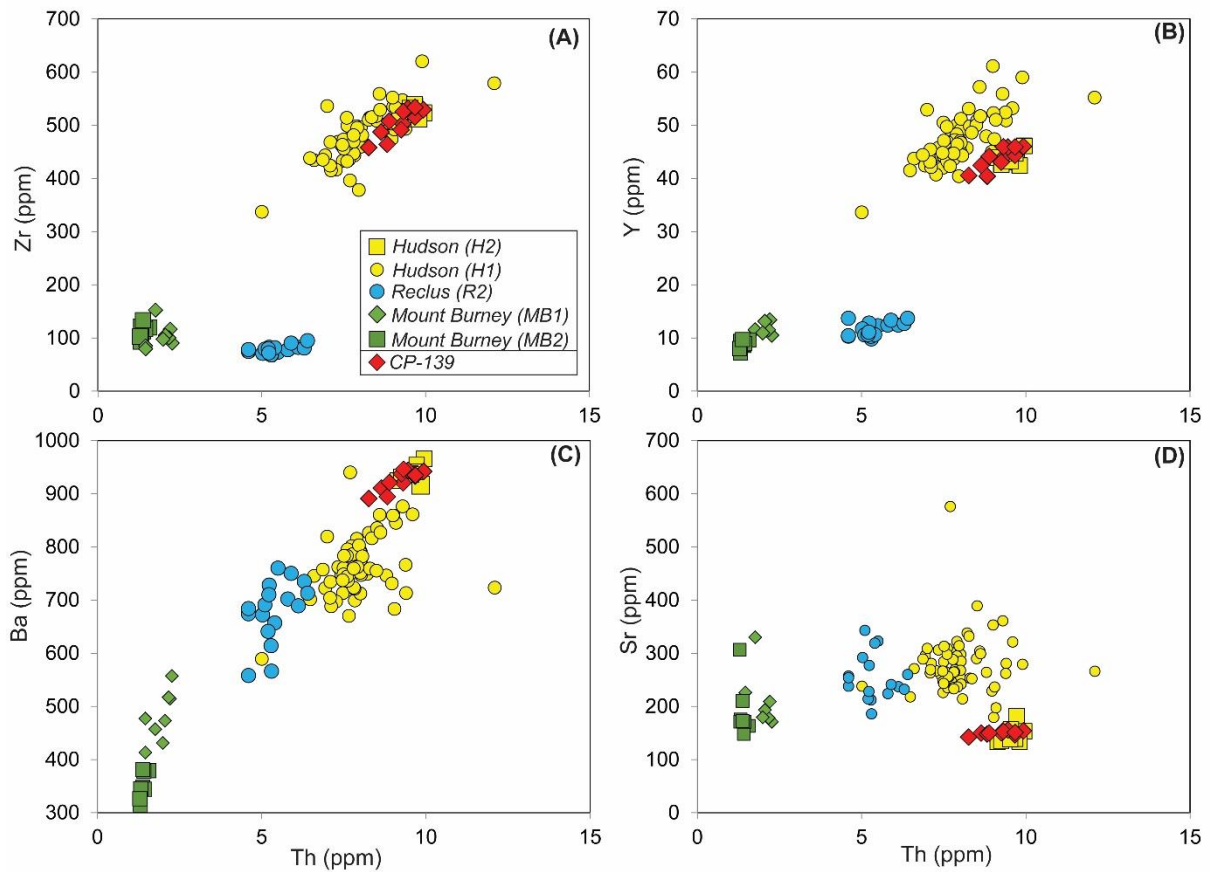
174 The SiO_2 content of the CP-139 glass shards is relatively low compared to those of known
175 widespread tephra units from large magnitude eruptions within the AVZ, for instance activity
176 at Mt. Burney, Reclus and Aguilera (**Fig. 3**). Furthermore, widespread tephra from Mt. Burney
177 and Reclus consist of glass compositions with a calc-alkaline affinity (CA; Smith et al., 2019)
178 inconsistent with the source of the CP-139 tephra. Further north in the SVZ of the Andes, a
179 number of volcanoes active during the Holocene have erupted HKCA deposits, including
180 Quatrupillian, Sollipuli and Lanín (Fontijn et al., 2016). However, chronological inconsistency
181 combined with a clear offset to higher Na_2O content in the CP-139 glass shards, relative to the
182 products of these volcanoes at overlapping SiO_2 content, clearly preclude any potential
183 correlations.

184 The CP-139 glass shards are indistinguishable at a major element level from the HKCA
185 products of Hudson volcano in the SVZ, and specifically the mid-Holocene Hudson-2 (H2)
186 that was chemically characterised in Smith et al., (2019). Near-source (55 km NE) H2 major
187 element glass data reported in Smith et al., (2019) was generated from ash layers preserved in
188 Lago Quijada and Lago Espejo that were identified by Weller et al., (2015). To test the strength
189 of our major element correlation, we compared trace elements concentrations from CP-139
190 glass shards to new grain-specific data produced here for the H2 tephra at Lago Quijada. Trace
191 element concentrations observed in CP-139 are consistent with the H2 tephra at Lago Quijada
192 (**Fig. 4**) and can be clearly distinguished from the less enriched incompatible trace element

193 contents (e.g., Th, Y, Zr) of widespread tephra units erupted within the AVZ (De Carlo et al.,
 194 2018).



195
 196 **Figure 3.** Major element biplots comparing major elements of individual glass shards of CP-139 cryptotephra and
 197 widespread Holocene-Late Glacial tephra units originating from the volcanoes of the AVZ (Mt. Burney [MB1],
 198 Reclus [R1] and Aguilera [A1]) and the SVZ, (Hudson-1 [H1] and Hudson-2 [H2]) (data from Smith et al., 2019).
 199 Also shown are glass compositions of HKCA tephra layers from volcanoes located further north in the Southern
 200 Volcanic Zone including Chaitén, Lanín, Quetrupillan and Sollipulli (Fontijn et al., 2016). (A) Total alkali vs.
 201 Silica diagram follows Le Bas et al., (1986) and (B) SiO₂ vs K₂O classification diagram following Percerillo and
 202 Taylor (1976). Glass data presented has been normalized to 100 wt%, and error bars represent 2 standard
 203 deviations of repeat analyses of the StHs6/80-G secondary standard.



204

205 **Figure 4.** Trace element biplots showing the concentrations of individual glass shards from the CP-139
 206 cryptotephra (Falkland Islands), the mid-Holocene Hudson-2 (H2; Lago Quijada). Also shown are the trace
 207 element concentrations of the Hudson-1 (H1), Mt. Burney-1 (MB1), Mt. Burney-2 (MB2), and Reclus-2 (R2)
 208 tephra deposits, which relate to the Del Carlo et al., (2018) EO-2L, EO-2D, EO-1b and LA-IB samples. 2 x
 209 standard deviation error bars associated with repeat analyses of the StHs6/80-G secondary standard run alongside
 210 the CP-139 and H2 samples are typically smaller than the data symbols.

211

212

213

214

215

216 **3.3 Implications**

217 *3.3.1 Distribution of the H2 tephra*

218 The occurrence of H2 as a cryptotephra in the Falkland Islands (1280 km SE of Mount Hudson)
219 significantly extends the previously known distribution of this marker horizon (Fig 1). The
220 first detailed report of H2 deposits by Naranjo and Stern (1998) showed an easterly dispersal
221 with thicknesses that ranged from 40 cm at 55 km from the volcano, to <5 cm at 90 km from
222 Mt. Hudson. H2 is widespread (>10 cm-thick) near the city of Coyhaique (80 km NE; sites 9-
223 21 in Fig. 1) and has been reported 140 km to the SSE near Cochrane (<2 cm-thick; sites 5-8
224 in Fig. 1). H2 tephra has also been reported (>5 cm thick layers) at several distant sites,
225 including the Los Toldos, Cerro Tres Tetas and Cueva de la Ventana archaeological sites 350
226 to 430 km SE (sites 23-25 in Fig. 1).

227 *3.3.2 Dispersal and spatial extent of the H2 tephra*

228 The occurrence of H2 ash in the Falkland Islands also indicates that the widespread distribution
229 of H2 ash by high altitude winds may have been in a more SE direction than previously
230 reported. According to Naranjo and Stern (1998), the dispersal axis of tephra fall from the H2
231 eruption, inferred from near-source deposits, was predominantly in an easterly direction
232 (N85°E). Distal transport of volcanic ash towards the Falkland Islands (SE) may therefore seem
233 inconsistent with this dispersal axis. However, distal transport to the SE is also supported by
234 the reported H2 occurrences in the localities of Los Toldos, Cerro Tres Tetas and Cueva de la
235 Ventana (Fig. 1). These sites are also directly in line with the SE distribution of the Hudson
236 1991 tephra (Scasso et al., 1994). H2 deposits at these sites are > 5cm, which is similar to or
237 greater than the thickness of the 1991 tephra that fell at these localities, according to the
238 isopachs drawn by Scasso et al., (1994). This and the occurrence of H2 ash in the Falklands
239 suggests that distal distribution of H2 tephra to the SE was as great, if not greater than during
240 the 1991 eruption.

241 Dispersal mechanisms and synoptic wind conditions similar to those observed during the 1991
242 Hudson eruption may also help explain the delivery of H2 ash fall to the Falkland Islands.
243 Satellite observations and simulations of phase II of the 1991 eruption indicate the ash plume
244 was initially directed to the south before moving to the east and settling into a fixed SE direction
245 (Kratzmann et al., 2010; Constantine et al., 2000). At its peak, the plume was elongated (1500
246 km SE) and reached a width of 370 km over the Falkland Islands (Scasso et al., 1994). High
247 velocity westerly winds in the jet stream resulted in a relatively confined plume and long-range
248 distal transport of ash (Scasso et al., 1994). Similar mechanisms observed during the 1991
249 eruption may account for both an easterly dispersal axis near the source and long-range distal
250 southern transport of fine H2 ash over the Falkland Islands. Given the high concentrations of
251 glass shards, H2 tephra is likely to be present throughout South Eastern Patagonia and may
252 even extend to the Southern Ocean and the fringes of Antarctica as a cryptotephra.

253 *3.3.3 Age of the H2 eruption*

254 According to our age-depth model, the H2 tephra is slightly older (4265 ± 65 cal BP) than
255 previously reported age estimates (Naranjo and Stern, 1998). Our age depth model derived
256 from terrestrial plant macrofossils likely provides a more accurate age for the H2 eruption.
257 Dating short-lived terrestrial plant remains ensures that the assimilated atmospheric CO₂ is
258 near-contemporaneous with the terrestrial environment, reflecting time of deposition (Lowe
259 and Walker, 1997; Turney et al., 2000). In addition, a site location with minimal opportunities
260 for redeposition such as a local topographic peak (e.g. Canopus Hill) provides an important
261 basis of a robust chronology (Thomas et al., 2019).

262 In contrast, bulk sediment, that forms the majority of previous dating, may incorporate root
263 material or downward vertical migration of microfossils by water movement/flow, both of
264 which would result in a younger radiocarbon age determination. The commonly cited age of
265 the H2 eruption (3600 BP; ~3.9 ka cal BP) was derived from ¹⁴C ages of organic soil, sediment

266 and bulk peat bracketing the tephra (Naranjo and Stern, 1998; Weller et al., 2018). Other age-
267 estimates of the H2 eruption have been extrapolated from lake sediment cores using bulk
268 radiometric dates and the total organic fraction of bulk sediment samples (e.g. Haberle and
269 Lumley, 1998; Elbert et al., 2013).

270 Given this older age of 4265 ± 65 cal BP, the H2 tephra may provide a key marker horizon for
271 the Middle–Late Holocene Boundary (4.2 ka BP; Walker et al., 2012), an important
272 climatostratigraphic boundary for which there are limited absolute time markers across the
273 Southern Hemisphere. In South America, it marks the end of a period of widespread aridity
274 that resulted in population decline and/or collapse (Riris and Arroyo-Kalin, 2019). The H2
275 cryptotephra may therefore provide an important isochron for terrestrial and marine studies
276 across Patagonia and Tierra del Fuego during a period of significant palaeoclimatic and
277 prehistoric societal change across this region.

278 **4. Conclusion**

279 The identification of a distal trachydacite-rhyolitic cryptotephra (CP-139) from the H2 eruption
280 in the Falkland Islands greatly increases the previously known distribution of this key marker
281 horizon. The high concentration of glass shards in our peat sequence suggests that the tephra
282 may be more widespread than presently understood and may serve as an important isochron
283 for the South Atlantic Ocean and also possibly Antarctica. Our reference dataset of major and
284 trace element glass composition can be used to identify the H2 tephra in other distal locations
285 and is an important contribution in the development of a regional framework for the
286 tephrostratigraphy of Patagonia. Finally, this research sets a precedent for further work into
287 identifying South American cryptotephra in the sedimentary records of the Falkland Islands.

288

289

290 **Acknowledgements**

291 This project was supported by the Australian Research Council (grant no. DE200100907 and
292 DP130104156). P. Panaretos was supported by a UNSW Summer Vacation Research
293 Scholarship. P.G.A and G.J are funded through a UK Research and Innovation Future Leaders
294 Fellowship (MR/S035478/1). We thank Rebecca Smith for providing constructive comments
295 on an earlier version of this manuscript. We thank the Falkland Islands Government for
296 permission to undertake sampling on the island (permit number: R07/2011).

297 **Supporting Information**

298 **Figure S1.** Light microscope image of volcanic tephra shards from Canopus Hill (136-140
299 cm). Scale bar = 50 μ m

300 **Table S1.** Summary of previously reported H2 tephra.

301 **Table S2.** The chronological framework for the Canopus Hill peat sequence updated from
302 Thomas et al., (2018). Radiocarbon and modelled calibrated age ranges for the Canopus Hill
303 peat sequence.

304 **Text S1.** Major and trace element analysis of volcanic glass.

305 **Supplementary Data**

306 Glass compositional data, including means and two standard deviations, for both sample and
307 secondary glass standard measurements.

308 DOI will be created for the supplementary data upon submission

309

310 **Declaration of competing interests**

311 The authors declare no competing interests.

312

313

314

315

316

317 **Author contributions**

- 318 P. Panaretos: Conceptualization, Investigation, Data collection and Analysis, Writing –
319 original draft.
- 320 P. G. Albert: Conceptualization, data analysis, methodology, Writing - review & editing
- 321 Z. A. Thomas: Conceptualization, Supervision, Data analysis, Writing – review & editing
- 322 C. S.M. Turney: Conceptualization, Methodology, Supervision, Writing – review & editing
- 323 G. Jones: Data collection and analysis, Writing – review & editing
- 324 C. R. Stern: Data collection , resources, Writing - review & editing
- 325 A. N. Williams: Data collection, Writing - review & editing
- 326 V. C. Smith: Data collection, Writing - review & editing
- 327 A. G. Hogg: Data collection, Writing - review & editing
- 328 C. J. Manning: Data collection, Writing - review & editing

329

330 **References**

- 331 Alloway, B.V., Lowe, D.J., Larsen, G., Shane, P.A.R., Westgate, J.A., 2013. Tephrochronology. In:
332 Elias, S.A., Mock, C.J. (ed.), *The Encyclopaedia of Quaternary Science* (second ed.) 4: 277-304.
333 Elsevier, Amsterdam
- 334 Blockley, S.P.E., Pyne-O'Donnell, S.D.F., Lowe, J.J., Matthews, I.P., Stone, A., Pollard, A.M., Turney,
335 C.S.M., Molyneux, E.G., 2005. A new and less destructive laboratory procedure for the physical
336 separation of distal glass tephra shards from sediments. *Quaternary Science Reviews* 24(16-17),
337 1952-1960. <https://doi.org/10.1016/j.quascirev.2004.12.008>
- 338 Bronk Ramsey, C., 2017. OxCal Program Version 4.3.
- 339 Bronk Ramsey, C., 2008. Deposition models for chronological records. *Quaternary Science Reviews*
340 27, 42–60. <https://doi.org/10.1016/j.quascirev.2007.01.019>
- 341 Bronk Ramsey, C., 2009. Dealing with outliers and offsets in radiocarbon dating. *Radiocarbon* 51,
342 1023–1045. <https://doi.org/10.1017/S0033822200034093>
- 343 Bronk Ramsey, C., Lee, S., 2013. Recent and Planned Developments of the Program OxCal.
344 *Radiocarbon* 55, 720–730. https://doi.org/10.2458/azu_js_rc.55.16215
- 345 Cardich, A.R., 1984-1985. Una fecha radiocarbónica más de la Cueva 3 de Los Toldos, Santa Cruz.
346 *Relaciones de la Sociedad Argentina de Antropología* 16, 269-273
- 347 Clark R, Wilson P., 1992. Occurrence and significance of ventifacts in the Falkland Islands, South
348 Atlantic. *Geografiska Annaler* 74A:35–46. <https://doi.org/10.1080/04353676.1992.11880347>
- 349 Constantine, E.K., Bluth, G.J.S., Rose, W.I., 2000. TOMS and AVHRR Observations of Drifting
350 Volcanic Clouds From the August 1991 Eruptions of Cerro Hudson. In: P. Mouginis-Mark, J.

- 351 Crisp, & J. Fink (eds.). Remote Sensing of Active Volcanism, 45–64. Washington, DC:
352 Geophysical Monograph
- 353 Del Carlo, P., Di Roberto, A., D'Orazio, M., Petrelli, M., Angioletti, A., Zanchetta, G., Maggi, V., Daga,
354 R., Nazzari, M., Rocchi, S., 2018. Late Glacial-Holocene tephra from southern Patagonia and
355 Tierra del Fuego (Argentina, Chile): A complete textural and geochemical fingerprinting for distal
356 correlations in the Southern Hemisphere. *Quaternary Science Reviews* 195, 153-170.
357 <https://doi.org/10.1016/j.quascirev.2018.07.028>
- 358 Dugmore, A. J., 1989. Icelandic volcanic ash in Scotland. *Scottish Geographical Magazine* 105, 168–
359 172. <https://doi.org/10.1080/14702548908554430>
- 360 Dunbar, N.W., Iverson, N.A., Van Eaton, A.R., Sigl, M., Alloway, B.V., Kurbatov, A.V., Mastin, L.G.,
361 McConnell, J.R., Wilson, C.J.N., 2017. New Zealand supereruption provides time marker for the
362 Last Glacial Maximum in Antarctica. *Scientific Reports* 7:12238. [https://doi.org/10.1038/s41598-
363 017-11758-0](https://doi.org/10.1038/s41598-017-11758-0)
- 364 Elbert, J., Wartenburger, R., von Gunten, L., Urrutia, R., Fischer, D., Fujak, M., Hamann, Y., Greber,
365 N.D., Grosjean, M., 2013. Late Holocene air temperature variability reconstructed from the
366 sediments of Laguna Escondida, Patagonia, Chile (45°30'S). *Palaeogeography,*
367 *Palaeoclimatology, Palaeoecology* 369, 482– 492. <https://doi.org/10.1016/j.palaeo.2012.11.013>
- 368 Fagel, N., Alvarez, D., Namur, O., Devidal, J.L., Nuttin, L., Schmidt, S., Jana, P., Torrejon, F., Bertrand,
369 S., Araneda, A., Urrutia, R., 2017. Lacustrine record of last millennia eruptions in Northern
370 Chilean Patagonia (45–47° S). *The Holocene* 27(8), 1227-1251.
371 <https://doi.org/10.1177/0959683616687380>
- 372 Fontijn, K., Rawson, H., Van Daele, M., Moernaut, J., Abarzúa, A.M., Heirman, K., Bertrand, S., Pyle,
373 D.M., Mather, T.A., De Batist, M., Naranjo, J.A., 2016. Synchronisation of sedimentary records
374 using tephra: A postglacial tephrochronological model for the Chilean Lake District. *Quaternary*
375 *Science Reviews* 137, 234-254. <http://dx.doi.org/10.1016/j.quascirev.2016.02.015>
- 376 Fontijn, K., Lachowycz, S.M., Rawson, H., Pyle, D.M., Mather, T. A., Naranjo, J.A., Moreno-Roa, H.,
377 2014. Late Quaternary tephrostratigraphy of southern Chile and Argentina. *Quaternary Science*
378 *Reviews* 89, 70–84. <https://doi.org/10.1016/j.quascirev.2014.02.007>
- 379 Global Volcanism Program., 2020. Smithsonian Institution. <https://volcano.si.edu/>, accessed date: 13
380 November 2020
- 381 Haberle, S.G., Lumley, S.H., 1998. Age and origin of tephras recorded in postglacial lake sediments to
382 the west of the southern Andes, 44°S to 47°S. *Journal of Volcanology and Geothermal Research*
383 84, 239-256. [https://doi.org/10.1016/S0377-0273\(98\)00037-7](https://doi.org/10.1016/S0377-0273(98)00037-7)
- 384 Hall, V. A., Wilson, P., Holmes, J., 2001. A preliminary tephra study of Holocene peats in the Falkland
385 Islands. *Dossiers de l'Archéol-Logis* 1, 39–44.
- 386 Hogg, A.G., Heaton, T.J., Hua, Q., Palmer, J.G., Turney, C.S.M., Southon, J., Bayliss, A., Blackwell,
387 P.G., Boswijk, G., Ramsey, C.B., Pearson, C., 2020. SHCal20 Southern Hemisphere calibration,
388 0–55,000 years cal BP. *Radiocarbon* 62(4), 759-778. <https://doi.org/10.1017/RDC.2020.59>
- 389 Hua, Q., Barbetti, M., Rakowski, A.Z., 2013. Atmospheric Radiocarbon for the Period 1950–2010.
390 *Radiocarbon* 55, 2059–2072. http://doi.org/10.2458/azu_js_rc.v55i2.16177

- 391 Jochum, K.P., Stoll, B., Herwig, K., Willbold, M., Hofmann, A.W., Amini, M., Aarburg, S.,
392 Abouchami, W., Hellebrand, E., Mocek, B., Raczek, I., 2006. MPI-DING reference glasses for in
393 situ microanalysis: New reference values for element concentrations and isotope ratios.
394 *Geochemistry, Geophysics, Geosystems* 7(2). <https://doi.org/10.1029/2005GC001060>
- 395 Kearney, R., Albert, P.G., Staff, R.A., Pál, I., Veres, D., Magyari, E., Ramsey, C.B., 2018. Ultra-distal
396 fine ash occurrences of the Icelandic Askja-S Plinian eruption deposits in Southern Carpathian
397 lakes: New age constraints on a continental scale tephrostratigraphic marker. *Quaternary Science*
398 *Reviews* 188, 174-182. <https://doi.org/10.1016/j.quascirev.2018.03.035>
- 399 Kilian, R., Hohner, M., Biester, H., Wallrabe-Adams, H.J., Stern, C.R., 2003. Holocene peat and lake
400 sediment tephra record from the southernmost Chilean Andes (53-55 degrees S). *Revista*
401 *Geologica De Chile* 30(1), 23-37. <http://dx.doi.org/10.4067/S0716-02082003000100002>
- 402 Kilian, R., Lamy, F., 2012. A review of Glacial and Holocene paleoclimate records from southernmost
403 Patagonia (49-55°S). *Quaternary Science Reviews* 53, 1-23.
404 <https://doi.org/10.1016/j.quascirev.2012.07.017>
- 405 Lamy, F., Kilian, R., Arz, H.W., Francois, J.P., Kaiser, J., Prange, M., Steinke, T., 2010. Holocene
406 changes in the position and intensity of the southern westerly wind belt. *Nature Geoscience* 3(10),
407 695-699. <https://doi.org/10.1038/ngeo959>
- 408 Kratzmann, D.J., Carey, S.N., Fero, J., Scasso, R.A., Naranjo, J.A., 2010. Simulations of tephra
409 dispersal from the 1991 explosive eruptions of Hudson volcano, Chile. *Journal of Volcanology*
410 *and Geothermal Research* 190, 337-352. <http://doi.org/10.1016/j.jvolgeores.2009.11.021>
- 411 Lane, C.S., Lowe, D.J., Blockley, S.P.E., Suzuki, T., Smith, V.C., 2017. Advancing tephrochronology
412 as a global dating tool: applications in volcanology, archaeology, and paleoclimatic research.
413 *Quaternary Geochronology* 40, 1-7. <http://dx.doi.org/10.1016/j.quageo.2017.04.003>
- 414 Le Bas, M.J., Le Maitre, R.W., Streckeisen, A., Zanettin, B., 1986. A chemical classification of volcanic
415 rocks based on the total alkali-silica diagram. *Journal of Petrology* 27, 745-750.
416 <https://doi.org/10.1093/petrology/27.3.745>
- 417 Lowe, D.J., 2011. Tephrochronology and its application: A review. *Quaternary Geochronology* 6, 107-
418 153. <https://doi.org/10.1016/j.quageo.2010.08.003>
- 419 Lowe, J.J., Walker, M.J.C., 1997. *Reconstructing Quaternary Environments*, 2nd Edition. ed.
420 Routledge.
- 421 Markgraf, V., Whitlock, C., Haberle, S., 2007. Vegetation and fire history during the last 18,000 cal yr
422 B.P. in Southern Patagonia: Mallín Pollux, Coyhaique, Province Aisén (45°41'30" S, 71°50'30"
423 W, 640 m elevation). *Palaeogeography, Palaeoclimatology, Palaeoecology* 254, 492-507.
424 <https://doi.org/10.1016/j.palaeo.2007.07.008>
- 425 Monteath, A.J., Hughes, P.D.M., Wastegård, S., 2019. Evidence for distal transport of reworked Andean
426 tephra: Extending the cryptotephra framework from the Austral volcanic zone. *Quaternary*
427 *Geochronology* 51, 64-71. <https://doi.org/10.1016/j.quageo.2019.01.003>
- 428 Moreno, P.I., Vilanova, I., Villa-Martínez, R., Garreaud, R.D., Rojas, M., De Pol-Holz, R., 2014.
429 Southern Annular Mode-like changes in southwestern Patagonia at centennial timescales over the
430 last three millennia. *Nature Communications* 5, 4375. <https://doi.org/10.1038/ncomms5375>

- 431 Naranjo, J.A., Stern, C.R., 1998. Holocene explosive activity of Hudson volcano, Southern Andes.
432 Bulletin of Volcanology 59, 291–306. <https://doi.org/10.1007/s004450050193>
- 433 Oppedal, L.T., van der Bilt, W.G., Balascio, N.L., Bakke, J., 2018. Patagonian ash on sub-Antarctic
434 South Georgia: expanding the tephrostratigraphy of southern South America into the Atlantic
435 sector of the Southern Ocean. Journal of Quaternary Science 33(5), 482-486.
436 <http://doi.org/10.1002/jqs.3035>
- 437 Otley, H., Munro, G., Clausen, A., Ingham, B. (2008). Falkland Islands state of the environment report
438 2008. Falkland Islands Government and Falklands Conservation, Stanley
- 439 Paunero, R. S., 2000. Canadon Cueva de la Ventana: tefras del Holocene medio. In: Guia de camo de
440 la visita a las localidades arqueologicas: La colonizacion del sur de America durante la tansicion
441 Pleitoceno/Holoceno. (L. Miotti, R.S. Paunero, M Salemm, G.R. Cattaneo, Eds), Chapter 6.4,
442 113-118.
- 443 Paunero, R.S., 1993-94. El sitio Cueva 1 de la localidad arqueologica Cerro Tres Tetras (Estancia San
444 Rafael, provincial de Santa Cruz, Argentina). Anales de Arqueologia y Etnologia, 48:49, 3-90
- 445 Pearce, N.J., Alloway, B.V., Westgate, J.A., 2008. Mid-Pleistocene silicic tephra beds in the Auckland
446 region, New Zealand: their correlation and origins based on the trace element analyses of single
447 glass shards. Quaternary International 178, 16-43. <https://doi.org/10.1016/j.quaint.2006.09.005>
- 448 Peccerillo, A., Taylor, S.R., 1976. Geochemistry of Eocene calcalkaline volcanic rocks from
449 Kastamonu area, Northern Turkey. Contributions to Mineralogy and Petrology 58, 39–63.
450 <https://doi.org/10.1007/BF00384745>
- 451 Pilcher, J. R., Hall, V. A., 1992. Towards a tephrochronology for the Holocene of the north of Ireland.
452 The Holocene 2, 255–259. <https://doi.org/10.1177%2F095968369200200307>
- 453 Riris, P., Arroyo-Kalin, M., 2019. Widespread population decline in South America correlates with
454 mid-Holocene climate change. Scientific reports 9, 6850. <https://doi.org/10.1038/s41598-019-43086-w>
455
- 456 Scasso, R.A., Corbella, H., Tiberi, P., 1994. Sedimentological analysis of the tephra from the 12–15
457 August 1991 eruption of Hudson volcano. Bulletin of Volcanology 56, 121–132.
458 <https://doi.org/10.1007/BF00304107>
- 459 Smith, R.E., Smith, V.C., Fontijn, K., Gebhardt, A.C., Wastegård, S., Zolitschka, B., Ohlendorf, C.,
460 Stern, C., Mayr, C., 2019. Refining the Late Quaternary tephrochronology for southern South
461 America using the Laguna Potrok Aike sedimentary record. Quaternary Science Reviews 218,
462 137-156. <https://doi.org/10.1016/j.quascirev.2019.06.001>
- 463 Smith, V.C., Costa, A., Aguirre-Díaz, G., Pedrazzi, D., Scifo, A., Plunkett, G., Poret, M., Tournigand,
464 P.Y., Miles, D., Dee, M.W., McConnell, J.R., 2020. The magnitude and impact of the 431 CE
465 Tierra Blanca Joven eruption of Ilopango, El Salvador. Proceedings of the National Academy of
466 Sciences 117(42), 26061-26068.
- 467 Stern, C.R., 2004. Active Andean volcanism: its geologic and tectonic setting. Revista Geológica de
468 Chile, 31(2), 1–51. <https://doi.org/10.4067/S0716-02082004000200001>.

- 469 Stern, C.R., 2008. Holocene tephrochronology record of large explosive eruptions in the southernmost
470 Patagonian Andes. *Bulletin of Volcanology* 70, 435–454. [http://doi.org/10.1007/s00445-007-](http://doi.org/10.1007/s00445-007-0148-z)
471 [0148-z](http://doi.org/10.1007/s00445-007-0148-z)
- 472 Stern, C.R., Moreno, P.I., Villa-Martinez, R., Sagredo, E.A., Prieto, A., Labarca, R., 2011. Evolution
473 of ice-dammed proglacial lakes in Última Esperanza, Chile: implications from the late-glacial R1
474 eruption of Reclús volcano, Andean Austral Volcanic zone. *Andean Geology* 38, 82–97.
- 475 Stern, C.R., Moreno Moncada, P., Henríquez, W.I., Villa Martínez, R., Sagredo, E., Aravena, J.C., Pol-
476 Holz, R.D., 2016. Holocene tephrochronology around Cochrane (~47° S), southern Chile. *Andean*
477 *Geology* 43(1), 1-19. <https://doi.org/10.5027/andgeoV43n1-a01>
- 478 Stern, C.R., Aguerre, A.M., Andrieu, J.M., 2019. Obsidian in the Dásovich rock-shelter, Chubut,
479 Argentina: Implications for long-distance acquisition behaviours. *Journal of Archaeological*
480 *Science: Reports* 28, 102028. <https://doi.org/10.1016/j.jasrep.2019.102028>
- 481 Thomas, Z. A., Jones, R.T., Fogwill, C.J., Hatton, J., Williams, A.N., Hogg, A., Mooney, S., Jones, P.,
482 Lister, D., Mayewski, P., Turney, C.S.M., 2018. Evidence for increased expression of the
483 Amundsen Sea Low over the South Atlantic during the late Holocene. *Climate of the Past* 14(11),
484 1727-1738. <https://doi.org/10.5194/cp-14-1727-2018>
- 485 Thomas, Z. A., Turney, C. S. M., Hogg, A. G., Williams, A. N., Fogwill, C. J., 2019. Investigating
486 subantarctic ¹⁴C ages of different peat components: site and sample selection for developing robust
487 age models in dynamic landscapes. *Radiocarbon* 61(4), 1009–1027.
488 <https://doi.org/10.1017/RDC.2019.54>
- 489 Tomlinson, E.L., Thordarson, T., Müller, W., Thirlwall, M., Menzies, M.A., 2010. Microanalysis of
490 tephra by LA-ICP-MS—strategies, advantages and limitations assessed using the Thorsmörk
491 Ignimbrite (Southern Iceland). *Chemical Geology* 279(3-4), 73-89.
492 <https://doi.org/10.1016/j.chemgeo.2010.09.013>
- 493 Turney, C.S.M., Jones, R. T., Fogwill, C., Hatton, J., Williams, A. N., Hogg, A., Thomas, Z. A., Palmer,
494 J., Mooney, S., Reimer, R.W., 2016. A 250-year periodicity in Southern Hemisphere westerly
495 winds over the last 2600 years. *Climate of the Past* 12, 189–200. [https://doi.org/10.5194/cp-12-](https://doi.org/10.5194/cp-12-189-2016)
496 [189-2016](https://doi.org/10.5194/cp-12-189-2016)
- 497 Turney, C.S.M., Lowe, J.J., 2001. Tephrochronology. In: Last, W.M., Smol, J.P. (Eds.), *Tracking*
498 *Environmental Change Using Lake Sediments: Physical and Chemical Techniques*. Kluwer
499 Academic Press, Dordrecht, The Netherlands, 451–471.
- 500 Turney, C.S.M., Coope, G.R., Harkness, D.D., Lowe, J.J., Walker, M.J.C., 2000. Implications for the
501 dating of Wisconsinan (Weichselian) Late-glacial events of systematic radiocarbon age
502 differences between terrestrial plant macrofossils from a site in SW Ireland. *Quaternary Research*
503 53, 114–121. [doi:10.1006/qres.1999.2087](https://doi.org/10.1006/qres.1999.2087)
- 504 Turney et al., (in review) - Chris Turney, Lorena Becerra-Valdivia, Adam Sookdeo, Zoë A. Thomas,
505 Jonathan Palmer, Heather A. Haines, Haidee Cadd, Lukas Wacker, Andy Baker, Martin S.
506 Andersen, Geraldine Jacobsen, Karina Meredith, Khorshed Chinu and Christopher Marjo (in
507 review), *Radiocarbon Protocols and First Intercomparison Results from the Chronos ¹⁴Carbon-*
508 *Cycle Facility, University of New South Wales, Sydney, Australia. Radiocarbon.*

- 509 Upton, J., Shaw C.J., 2002. An overview of the oceanography and meteorology of the Falkland Islands.
510 Aquatic conservation. Marine and Freshwater Ecosystems 12, 15–
511 25. <https://doi.org/10.1002/aqc.496>
- 512 Walker, M.J.C., Berkelhammer, M., Björck, S., Cwynar, L.C., Fisher, D.A., Long, A.J., Lowe, J.J.,
513 Newnham, R.M., Rasmussen, S.O., Weiss, H., 2012. Formal subdivision of the Holocene
514 Series/Epoch: a Discussion Paper by a Working Group of INTIMATE (Integration of ice-core,
515 marine and terrestrial records) and the Subcommittee on Quaternary Stratigraphy (International
516 Commission on Stratigraphy). Journal of Quaternary Science 27, 649-659.
517 <http://dx.doi.org/10.1002/jqs.2565>.
- 518 Wastegård, S., Turney, C.S.M., Lowe, J.J., Roberts, S.J., 2000. New discoveries of the Vedde Ash in
519 southern Sweden and Scotland. Boreas 29(1), 72-78.
- 520 Weller, D.J., Miranda, C.G., Moreno, P.I., Villa-Martínez, R., Stern, C.R., 2015. Tephrochronology of
521 the southernmost Andean southern volcanic zone, Chile. Bulletin of Volcanology 77, 1-24.
522 <https://doi.org/10.1007/s00445-015-0991-2>
- 523 Weller, D.J., de Porras, M.E., Maldonado, A., Méndez, C., Stern, C.R., 2018. New age controls on the
524 tephrochronology of the southernmost Andean Southern Volcanic Zone, Chile. Quaternary
525 Research 91(1), 250-264. <https://doi.org/10.1017/qua.2018.81>
- 526 Weller, D.J., Stern, C.R., 2018. Along-strike variability of primitive magmas (major and volatile
527 elements) inferred from olivine-hosted melt inclusions, southernmost Andean Southern Volcanic
528 Zone, Chile. Lithos 296–299, 233–244. <https://doi.org/10.1016/j.lithos.2017.11.009>.